Advances in Applied Mathematics and Mechanics
Adv. Appl. Math. Mech., Vol. **4**, No. 1, pp. 21-35

DOI: 10.4208/aamm.11-m1110
February 2012

The Sensitivity Analysis for the Flow Past Obstacles Problem with Respect to the Reynolds Number

Kazufumi Ito[1], Zhilin Li[1,2,*] and Zhonghua Qiao[3]

[1] *Center for Research in Scientific Computation & Department of Mathematics, North Carolina State University, Raleigh, NC 27695-8205, USA*
[2] *School of Mathematical Sciences, Nanjing Normal University, No. 1 Wenyuan Road, Yadong New District, Nanjing 210046, China*
[3] *Department of Mathematics, Hong Kong Baptist University, Kowloon Tong, Hong Kong*

Received 18 January 2011; Accepted (in revised version) 17 May 2011

Available online 13 December 2011

Abstract. In this paper, numerical sensitivity analysis with respect to the Reynolds number for the flow past obstacle problem is presented. To carry out such analysis, at each time step, we need to solve the incompressible Navier-Stokes equations on irregular domains twice, one for the primary variables; the other is for the sensitivity variables with homogeneous boundary conditions. The Navier-Stokes solver is the augmented immersed interface method for Navier-Stokes equations on irregular domains. One of the most important contribution of this paper is that our analysis can predict the critical Reynolds number at which the vortex shading begins to develop in the wake of the obstacle. Some interesting experiments are shown to illustrate how the critical Reynolds number varies with different geometric settings.

AMS subject classifications: 65M06, 65M12, 76T05

Key words: Navier-Stokes equations, sensitivity analysis, flow past cylinder, embedding technique, immersed interface method, irregular domain, augmented system, projection method, fluid-solid interaction.

1 Introduction

In [8], an augmented immersed interface method was proposed for the following non-dimensional incompressible Navier-Stokes equations on an irregular domain $R \setminus \Omega$:

$$\frac{\partial \mathbf{u}}{\partial t} + (\mathbf{u} \cdot \nabla)\mathbf{u} + \nabla p = \frac{1}{Re}\Delta \mathbf{u}, \qquad \mathbf{x} \in R \setminus \Omega, \tag{1.1a}$$

*Corresponding author.
URL: `http://www4.ncsu.edu/~zhilin/`
Email: kito@math.ncsu.edu (K. Ito), zhilin@math.ncsu.edu (Z. Li), zqiao@hkbu.edu.hk (Z. Qiao)

$$\nabla \cdot \mathbf{u} = 0, \qquad \mathbf{x} \in R \setminus \Omega, \tag{1.1b}$$

$$\mathbf{u}\big|_{\partial\Omega} = \mathbf{0}, \tag{1.1c}$$

$$\mathbf{u}(\mathbf{x}, 0) = \mathbf{u}_0, \qquad \text{IC}, \tag{1.1d}$$

with a usual flow boundary condition along ∂R, where R is a rectangular domain, see Fig. 1 for an illustration. In the above Navier-Stokes equations, $Re = 1/\mu$ is the Reynolds number and μ is the viscosity, $\mathbf{u}$ is the velocity, and Ω is a set of inclusions (obstacles), for example, one or two cylinders in this paper. We refer the readers to [8] and the references therein for detailed information about the problem and the related references. The method proposed in [8] is based on the augmented immersed interface method, see e.g., [9–13].

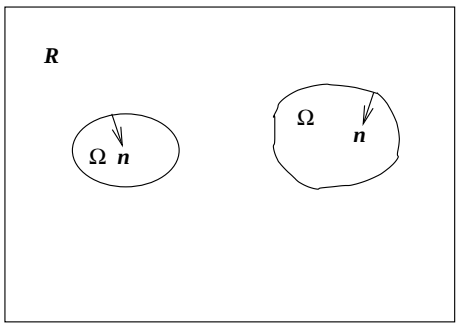

Figure 1: A diagram for the Navier-Stokes equations on an irregular domain.

In the literature, there are numerous papers on flow past cylinder problems. There are also a few of them that discuss the important quantities such as lift and drag coefficients (or forces), frequency of the vortex shading etc., as functions of the Reynolds number. In this paper, we are more interested in the sensitivity analysis with respect to the Reynolds number, or precisely $Re = 1/\mu$ when the obstacle is a circle. We believe that this paper is the first attempt to study the sensitivity of such a problem. Sensitivity analysis is important to understand how particular parameter(s) affect the solution behavior such as the stability of the flow, vortex shading behind the wake of the obstacles. As pointed out in [3], sensitivity analysis and uncertainty analysis combine to produce a systematic approach to develop a comprehensive understanding of a mathematical model, the data it produces, and the way that the data is used to influence the design of many engineering systems.

1.1 The sensitivity equations

In order to carry out the sensitivity analysis, we solve the sensitivity equations, see for example, [3, 6] and the reference therein:

$$\frac{\partial \mathbf{w}}{\partial t} + (\mathbf{u} \cdot \nabla)\mathbf{w} + (\mathbf{w} \cdot \nabla)\mathbf{u} + \nabla q = \frac{1}{Re}\Delta \mathbf{w} - \frac{1}{Re^2}\Delta \mathbf{u}, \qquad \mathbf{x} \in R \setminus \Omega, \tag{1.2a}$$

$$\nabla \cdot \mathbf{w} = 0, \qquad \mathbf{x} \in R \setminus \Omega, \tag{1.2b}$$

$$\mathbf{w}\big|_{\partial\Omega} = 0, \tag{1.2c}$$

$$\mathbf{w}(\mathbf{x}, 0) = 0, \qquad \text{IC}, \tag{1.2d}$$

with the same type as in (1.1a)-(1.1d) but homogeneous boundary condition along ∂R. The quantities $\mathbf{w}$ and $\nabla \times \mathbf{w}$ are called the sensitivity velocity and vorticity, and q is the sensitivity pressure. Sensitivity quantities are derivatives which describe how small change in design parameters affect the state variables of the mathematical model. We are particularly interested in the solution near the critical Reynolds number, for example, $Re \approx 47$ for a single cylinder, at which the vortex is about to develop.

The paper is organized as follows. In the next section, we will review the augmented immersed interface method for solving the Navier-Stokes solver on irregular domains and how to solve the sensitivity equations. In Section 3, we present our numerical experiments and analysis about the critical Reynolds number. Some conclusions and acknowledgments are followed in the last section.

2 The numerical algorithm

We use the augmented immersed interface method developed in [8] to solve the incompressible Navier-Stokes equations on an irregular domain $R \setminus \Omega$. The main ideas include extending the governing equations into the entire rectangular domain; introducing the jump in the normal derivative of the velocity as augmented variable with two components; and then employing the immersed interface method to solve the interface problem. The augmented variable is chosen so that the no-slip (or a given velocity such as rotating) boundary condition can be satisfied. The advantages of this approach include that, (1) the fast Poisson solver can be utilized in the Navier-Stokes solver via the modified projection method; (2) the condition number of the system of equations for the augmented variable is small compared with other approaches in the literature. For fixed obstacles or cylinders with fixed location but rotating, the coefficient matrix of the system of equations for the augmented variable is a constant matrix independent of time t and the mesh. In this case, only one LU decomposition is needed at the first time step.

We assume that the domain R is a rectangle $[a, b] \times [c, d]$ with holes Ω. The spatial spacing is chosen as

$$h_x = \frac{(b-a)}{M}, \qquad h_y = \frac{(d-c)}{N},$$

where M and N are the number of grid points in the x and y directions, respectively. We use a standard uniform Cartesian grid for simplicity. The time integration from t^k to t^{k+1} for the primary variables can be written as:

$$\frac{\mathbf{u}^* - \mathbf{u}^k}{\Delta t} + (\mathbf{u} \cdot \nabla \mathbf{u})^{k+\frac{1}{2}} = \begin{cases} -\nabla p^{k-\frac{1}{2}} + \dfrac{\mu}{2}\big(\Delta \mathbf{u}^* + \Delta \mathbf{u}^k\big), & \text{if } \mathbf{x} \in R \setminus \Omega, \\ \dfrac{\mu}{2}(\Delta \mathbf{u}^* + \Delta \mathbf{u}^k), & \text{if } \mathbf{x} \in \Omega, \end{cases} \tag{2.1a}$$

$$\mathbf{u}^*|_{\partial R} = \mathbf{u}_{\partial R}\big(\mathbf{x}, t^{k+1}\big), \tag{2.1b}$$

$$[\mathbf{u}^*]_{\partial\Omega}=0,\qquad \left[\frac{\partial \mathbf{u}^*}{\partial n}\right]_{\partial\Omega}=\boldsymbol{\psi}^{k+1},\qquad \mathbf{u}^*|_{\partial\Omega}=\mathbf{u}_{\partial\Omega}\big(\mathbf{x}_{\partial\Omega},t^{k+1}\big), \tag{2.1c}$$

$$\begin{cases} \Delta\phi^{k+1}=\dfrac{\nabla\cdot\mathbf{u}^*}{\Delta t}, & \mathbf{x}\in R,\\ \dfrac{\partial\phi^{k+1}}{\partial\mathbf{n}}\Big|_{\partial R}=0, \qquad \big[\boldsymbol{\phi}^{k+1}\big]_{\partial\Omega}=0, \qquad \left[\dfrac{\partial\boldsymbol{\phi}^{k+1}}{\partial n}\right]_{\partial\Omega}=0, \end{cases} \tag{2.1d}$$

$$\mathbf{u}^{k+1}=\mathbf{u}^*-\Delta t\nabla\phi^{k+1},\quad \mathbf{x}\in R, \tag{2.1e}$$

$$p^{k+\frac{1}{2}}=p^{k-\frac{1}{2}}+\phi^{k+1}, \tag{2.1f}$$

where $(\mathbf{u}\cdot\nabla\mathbf{u})^{k+1/2}$ is approximated by

$$(\mathbf{u}\cdot\nabla\mathbf{u})^{k+\frac{1}{2}}=\frac{3}{2}\big(\mathbf{u}^k\cdot\nabla\big)\mathbf{u}^k-\frac{1}{2}\big(\mathbf{u}^{k-1}\cdot\nabla\big)\mathbf{u}^{k-1}. \tag{2.2}$$

The projection method that we applied above is based on the methods described in [1, 2]. The projection method is second order accurate both in time and space.

We use the zero level set of a Lipschitz continuous function $\varphi(x,y)$, often the signed distance function, to represent the boundary of the obstacles, we refer the reader to [16,17] for more information about the level set functions and applications. One of advantages of this approach is that it can represent multi-connected domain easily as in our two cylinders case. In implementation, the level set function is defined at the grid points as $\varphi_{ij}=\varphi(x_i,y_j)$. Using a level set function, we can classify the grid points as regular or irregular ones. For a given grid point $\boldsymbol{x}=(x_i,y_j)$, we define

$$\varphi_{ij}^{\max}=\max\big\{\varphi_{i-1,j},\varphi_{i+1,j},\varphi_{ij},\varphi_{i,j-1},\varphi_{i,j+1}\big\}, \tag{2.3a}$$

$$\varphi_{ij}^{\min}=\min\big\{\varphi_{i-1,j},\varphi_{i+1,j},\varphi_{ij},\varphi_{i,j-1},\varphi_{i,j+1}\big\}. \tag{2.3b}$$

We call (x_i,y_j) an irregular grid point in reference to the central five point stencil if $\varphi_{ij}^{\max}\varphi_{ij}^{\min}\le 0$. For an irregular grid point, there exists an orthogonal projection $\boldsymbol{x}_p=(x_p,y_p)$ on the interface satisfying

$$\boldsymbol{x}_p=\boldsymbol{x}+\alpha\boldsymbol{n}(\boldsymbol{x}), \tag{2.4}$$

where α is to be determined and

$$\boldsymbol{n}=\frac{\nabla\varphi}{|\nabla\varphi|}, \tag{2.5}$$

is the unit normal direction at $\boldsymbol{x}$. The parameter α can be determined approximately by solving the following quadratic equation explicitly

$$\frac{1}{2}(\boldsymbol{n}^T\boldsymbol{H}\boldsymbol{n})\alpha^2+|\nabla\varphi|\alpha+\varphi(\boldsymbol{x})=0, \tag{2.6}$$

where $\boldsymbol{H}$ is the Hessian matrix

$$\boldsymbol{H}=\begin{pmatrix} \dfrac{\partial^2\varphi}{\partial x^2} & \dfrac{\partial^2\varphi}{\partial x\partial y}\\ \dfrac{\partial^2\varphi}{\partial x\partial y} & \dfrac{\partial^2\varphi}{\partial y^2}\end{pmatrix}. \tag{2.7}$$

All the quantities related to φ and its derivatives are evaluated at the grid point (x_i, y_j). The augmented variables are defined at the orthogonal projections from $\varphi \geq 0$ side, see also [4,5,7,15] for more details and other applications.

2.1 The augmented immersed interface method

In our method, we extend the Navier-Stokes equation to the entire rectangular domain so that a fast Poisson solver can be utilized. The original problem at one particular time step becomes an interface problem. The jump condition $[\partial \mathbf{u}^*/\partial \mathbf{n}]$ in the normal derivative of the velocity is used as an augmented variable. It is determined such that the boundary condition along $\partial\Omega$ are satisfied. This approach is described in more details below.

From time t^k to t^{k+1}, given an approximate jump $[\partial \mathbf{u}^*/\partial \mathbf{n}] = \psi^{k+1}$, or $\mathbf{Q}^{k+1}$ in the discrete form, the discrete solution $\mathbf{U}^*$ for $\mathbf{u}^*$ satisfies a linear system

$$A\mathbf{U}^* + B\mathbf{Q}^{k+1} = \mathbf{F}_1, \tag{2.8}$$

where the matrix A corresponds to the prediction step (2.1a)-(2.1c), and the vector $B\mathbf{Q}^{k+1}$ corresponds to the correction terms for the immersed interface method, see [14] due to the jump condition $[\partial \mathbf{u}^*/\partial n]_{\partial\Omega} = \psi^{k+1}$. The boundary condition (2.1c) (or the augmented equation) $\mathbf{u}^*|_{\partial\Omega} = \mathbf{u}_{\partial\Omega}^{k+1}$ is discretized via a least squares interpolation, and can be written in the discrete form

$$C\mathbf{U}^* + D\mathbf{Q}^{k+1} = \mathbf{U}_{\partial\Omega}^{k+1}. \tag{2.9}$$

If we put those two matrix-vector equations (2.8) and (2.9) together, we get

$$\begin{bmatrix} A & B \\ C & D \end{bmatrix} \begin{bmatrix} \mathbf{U}^* \\ \mathbf{Q}^{k+1} \end{bmatrix} = \begin{bmatrix} \mathbf{F_1} \\ \mathbf{U}_{\partial\Omega}^{k+1} \end{bmatrix}. \tag{2.10}$$

Note that the dimension of $\mathbf{Q}^{k+1}$ is $\mathcal{O}(2N)$ (assuming $M \sim N$), which is much smaller than that of $\mathbf{U}^*$ $(\mathcal{O}(2N^2))$.

Eliminating $\mathbf{U}^*$ from Eq. (2.10), we get the Schur-complement system for $\mathbf{Q}^{k+1}$;

$$(D - CA^{-1}B)\mathbf{Q}^{k+1} = \mathbf{U}_{\partial\Omega}^{k+1} - CA^{-1}\mathbf{F}_1 \stackrel{\text{def}}{=} \mathbf{F}_2, \quad \text{or } E\mathbf{Q}^{k+1} = \mathbf{F_2}. \tag{2.11}$$

Note that E is not symmetric in general. We can either use a direct method or an iterative method to solve the linear system (2.11) for $\mathbf{Q}^{k+1}$ depending on different situations. If the boundary $\partial\Omega$ is stationary and the time step is fixed, it is more efficient to use a direct method (say, Gaussian elimination with partial pivoting) since the coefficient matrix E is a constant matrix. Thus, we can form the coefficient matrix E explicitly by setting

$$\mathbf{Q}^{k+1,*} = e_\ell,$$

the ℓ-th unity vector, $l = 1, 2, \cdots$, and apply the LU decomposition to solve it directly. This is also advantageous for long time runs since the costly LU decomposition needs to be done just one time in the beginning.

Three Helmholtz/Poisson solvers are needed to evaluate $E\mathbf{Q}^{k+1}$ or $A^{-1}\mathbf{F}_1$. First, the prediction step for $\mathbf{u}^*$ requires a fast Helmholtz solver on a rectangular domain for each velocity component. Secondly, the projection step requires a fast Poisson solver for ϕ^{k+1} given $\mathbf{u}^*$. For stationary boundary $\partial\Omega$ and fixed time step Δt, all the matrices are constant matrices that depend on the fast Helmholtz/Poisson solver, and the interpolation scheme for the boundary condition.

2.2 Solving the sensitivity equations

For the sensitivity system (1.2a)-(1.2d), the numerical algorithm is almost the same. We still use the algorithm above for primary variable with homogeneous boundary condition of the same type and an non-homogeneous source term

$$-(\mathbf{u}\cdot\nabla\mathbf{w})^{k+\frac{1}{2}}-\big(\mathbf{w}\cdot\nabla\mathbf{u}\big)^{k+\frac{1}{2}}-\frac{1}{2}\mu^2\big(\Delta\mathbf{u}^{k+1}+\Delta\mathbf{u}^k\big), \tag{2.12}$$

in which $\mathbf{u}^{k+1}$ has already been calculated after we have solved the Navier-Stokes equations for the primary variables. The above expression is computed using the standard five-point stencil finite difference schemes at regular grid points, that is, all the grid points in the standard centered five-point stencil are from outside of the domain of the obstacles. For other grid points in the domain, a second order least square interpolation scheme is used to compute the source term.

3 Numerical experiments

In this section, we present some numerical results for the sensitivity analysis with respect to the Reynolds number $Re = 1/\mu$. All the computations were performed at the North Carolina State University using notebook or desktop computers.

The computer code has been validated in [8]. Thus we only show the results in our sensitivity analysis. In our problem set-up, we use a computational domain $[-10,10]\times[-5,5]$. The cylinders is either one or two circles/ellipses of the form

$$\frac{(x-x_0)^2}{a^2}+\frac{y^2}{b^2}=1,$$

which are represented by a level set function. We use a grid of 900 by 450 to get accurate results. The flow rate at $x=-10$ is one unit.

We measure the velocity and vorticity strength in the wake of the cylinder as follows

$$V_s(t)=\max_{\substack{x_1\le x\le x_2,\\ -4\le y\le 4}}\big|\mathbf{u}(\mathbf{x},t)\big|, \tag{3.1a}$$

$$\omega_s(t)=\max_{\substack{x_1\le x\le x_2,\\ -4\le y\le 4}}\big|\nabla\times\mathbf{u}(\mathbf{x},t)\big|. \tag{3.1b}$$

The velocity and vorticity are calculated outside the obstacles. In most of cases, we take $x_1 = -9.5$ and $x_2 = 9.5$. In this way, we exclude the effect of boundary on our analysis since we are more interested what is happening in the wake of obstacles.

3.1 A classical example: a single stationary cylinder

We first carry out the sensitivity analysis for a classical example, a uniform flow past a single stationary cylinder. The cylinder is represented by the level set function

$$\varphi(x,y) = \sqrt{(x+7)^2+y^2} - 1.$$

It is well-known that the critical Reynolds number for this case is around $47 \sim 48$.

In Fig. 2, we plot the velocity and vorticity strengths defined in (3.1a) and (3.1b) versus the Reynold number. We can see that the velocity and vorticity strengths behave roughly linearly for the primary velocity and vorticity from which there is not much information that we can extract from the plot about the critical Reynolds number. But the sensitivity variables have shown some important information after $Re \geq 45$. The magnitude of both the sensitivity velocity and vorticity are very small when $Re \leq 45$ indicating a uniform flow in the wake of the cylinder. After $Re \geq 45$, the magnitude of both the sensitivity velocity and vorticity increase rapidly. As we know that the vortexes will develop after the wake of the cylinder after $Re > 47$. Note that, the sensitivity vorticity strength actually decreases with the Reynolds number until some critical value Re^* before going up. The main finding of this paper is that Re^* is indeed a very good approximation of the critical Reynold number.

In Fig. 3, we plot the vorticity and sensitivity vorticity at time $t = 80$ with the Reynolds numbers $Re = 40, 50, 60, 80, 100$, and 150. The vorticity plots (top ones) are obtained with the contour option $-2.5 : 0.2 : 2.5$; The sensitivity vorticity are obtained

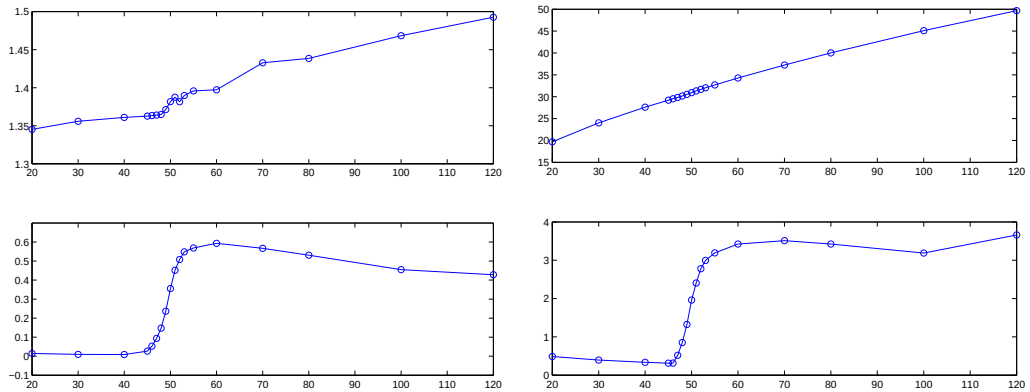

(a) (b)

Figure 2: (a) Plot of the velocity strength versus the Reynolds number defined in (3.1a). (b) Plot of the vorticity strength versus the Reynolds number defined in (3.1b). The top ones are for the primary velocity and vorticity while the bottom one are for the sensitivity equations.

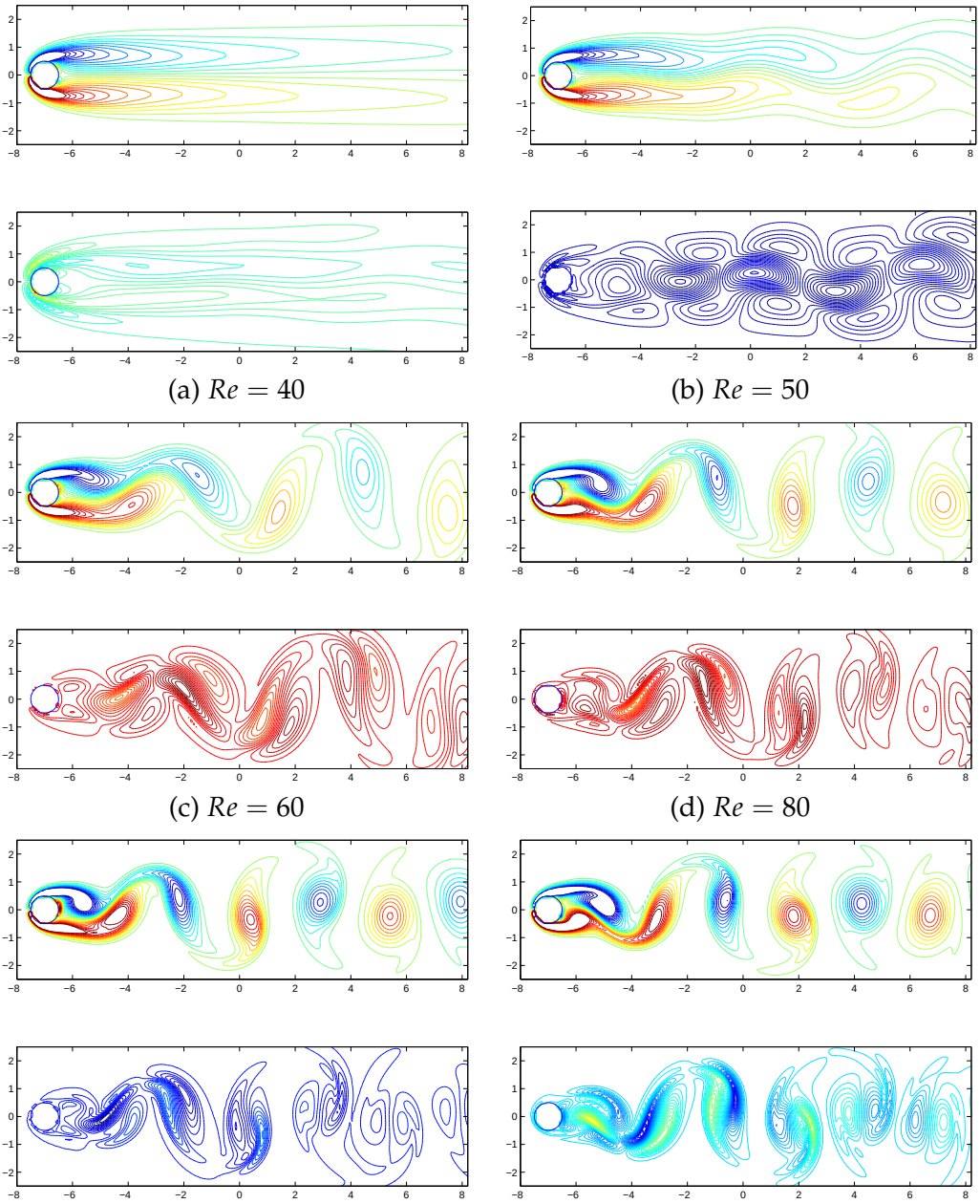

(a) $Re = 40$ (b) $Re = 50$

(c) $Re = 60$ (d) $Re = 80$

(e) $Re = 100$ (f) $Re = 110$

Figure 3: Contour plots of the vorticity and sensitivity vorticity at time $t = 80$ with the Reynolds numbers $Re = 40, 50, 60, 80, 100$ and 110. The vorticity plots (top ones) are obtained with the contour option $-2.5 : 0.2 : 2.5$. The sensitivity vorticity contour plot are obtained with $N = 80$ contour lines.

with the contour option contour, $-2.5 : 0.2 : 2.5$ or with N (say 80, 100, or 160) contour lines to have better visualization effect. From $Re = 45$ to $Re = 50$, the sensitivity vorticity strength increases significantly indicating that the vortex shading is about to

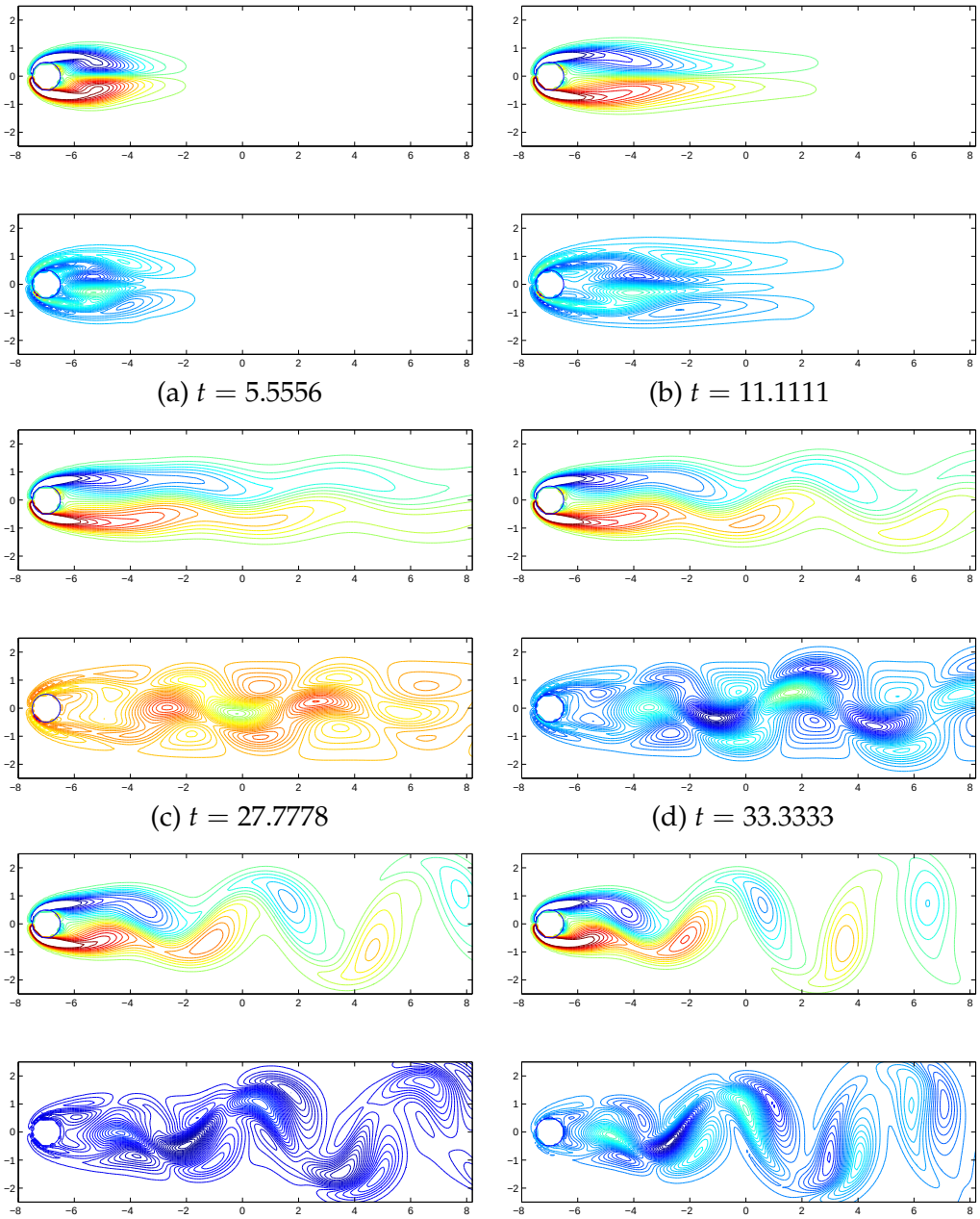

(a) $t = 5.5556$ (b) $t = 11.1111$

(c) $t = 27.7778$ (d) $t = 33.3333$

(e) $t = 44.4444$ (f) $t = 55.5556$

Figure 4: History of the vorticity and sensitivity vorticity with the Reynolds numbers $Re = 70$. The vorticity plots (top ones) are obtained with the contour option $-2.5 : 0.2 : 2.5$. The sensitivity vorticity contour plot are obtained using $N = 80$ contour lines.

develop. From $Re = 60$ to $Re = 100$, the sensitivity vorticity intensifies and a single vertex begin to split into two closed vortexes that behaves like a dipole. This can not be seen from the original vortexes.

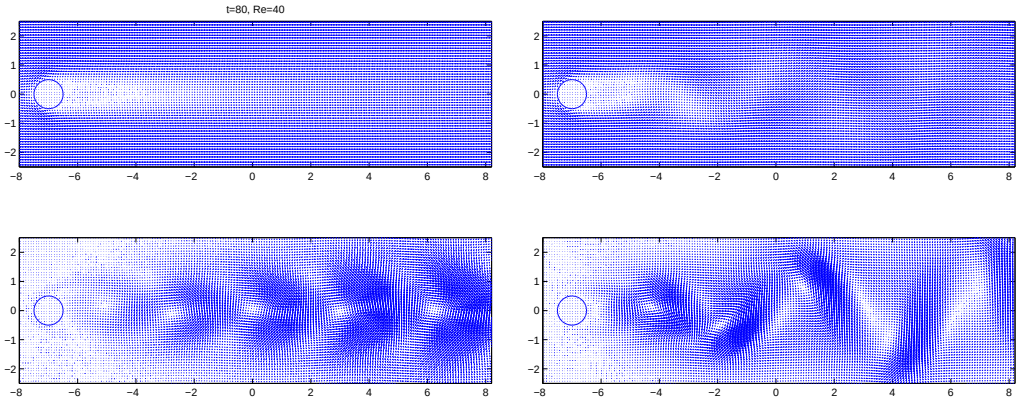

(a) $Re = 40$ (b) $Re = 60$

Figure 5: Plot of the velocity and the sensitivity velocity field at time $t = 80$: (a) $Re = 40$, (b) $Re = 60$. The top ones are the velocity while the bottom ones are sensitivity velocity.

In Fig. 4, we show the history of the vorticity and sensitivity vorticity at different time. From the plot, we can roughly see how the vortex sheets evolve with the time.

In Fig. 5, we plot the velocity and sensitivity velocity field at time $t = 80$ with $Re = 40$ and $Re = 60$. Again, we can see the vortex shading better from the sensitivity velocity. Even at $Re = 40$, we see something is about developing meaning a more unstable flow in the wake of the cylinder.

3.2 The effect of the shape and orientation of the obstacle on the vortex shading

In this experiment, we show similar analysis of flow past different obstacles. The obstacle that we are considering is an ellipse whose level set function is

$$\varphi(x,y) = \sqrt{\frac{(x+7)^2}{0.6^2} + \frac{y^2}{0.4^2}} - 1,$$

with different orientations. We see that critical Reynolds number of $Re^* = 1/\mu^*$ is quite different for different orientations. The sensitivity analysis does give a good estimate of the critical number at which the vortex shading is about to develop.

In Fig. 6, we show the sensitivity analysis of an ellipse at different orientations. The plots on the left are the plots of the vorticity (top) and sensitivity vorticity (bottom) strengths versus the parameter $1/\mu \sim Re$. From the plot, we can predict that the critical Reynolds number is significant different with the orientation. The results are also agree with intuition. With the orientation is parallel to the flow direction, the flow in the wake of the obstacle is more stable than that against the flow direction. As we can expected, we can predict that the critical Reynolds number is the largest for the horizontal case (around 70), decreases for the oblique ellipse (around 45), and the smallest for the vertical case (around 40). The plots on the right are vorticity (top) and sensitivity vorticity (bottom) at some numbers which supports our discussions above.

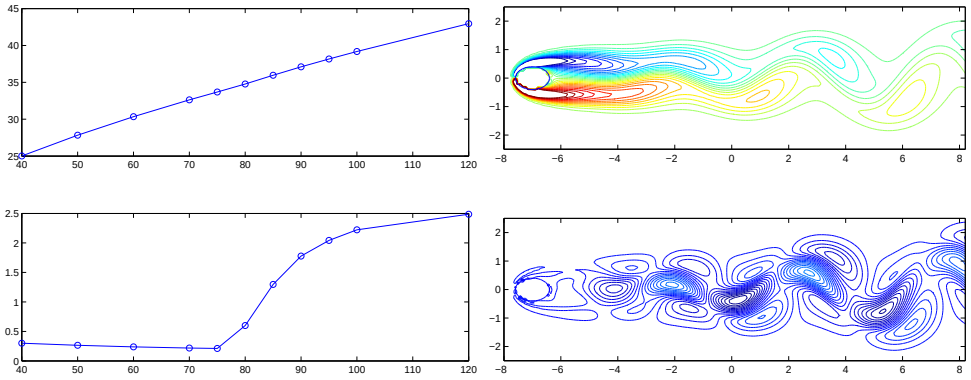

(a) Horizontal ellipse, the right plot are vorticity or sensitivity vorticity at $Re = 70$.

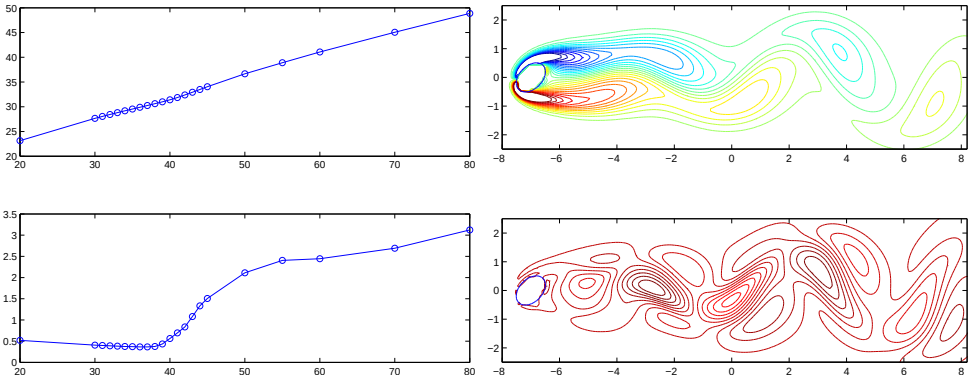

(b) Oblique ellipse, the right plot are vorticity or sensitivity vorticity at $Re = 45$.

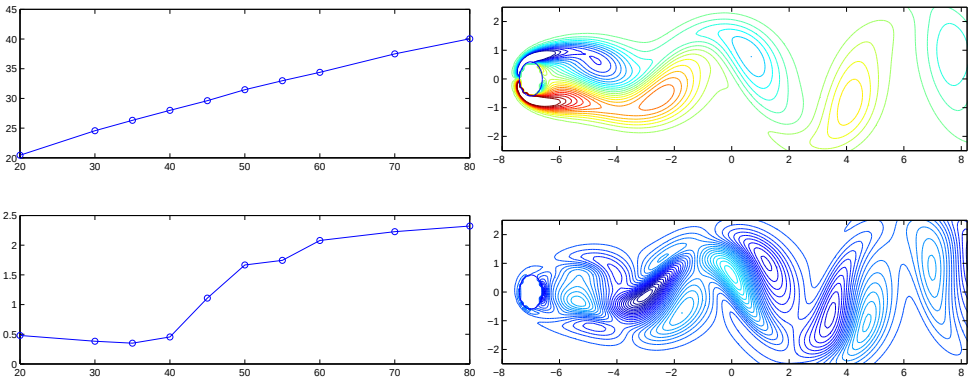

(c) Vertical ellipse, the right plot are vorticity or sensitivity vorticity at $Re = 40$.

Figure 6: Sensitivity analysis with an ellipse with major and minor axis being 0.6 and 0.4 at different orientations. (a) The major axes is aligned with the x-direction. (b) The ellipse is rotated forty-five degrees in counter-clock direction. (c) The major axes is aligned with the y-direction. The right plots are the vorticity when $1/\mu = 70, 45, 40$ respectively.

3.3 A rotating cylinder

We carry out the sensitivity analysis for a rotating cylinder in the uniform flow. The cylinder is rotating counter clockwise in a constant velocity $(-0.25, 0.25)$. Since the

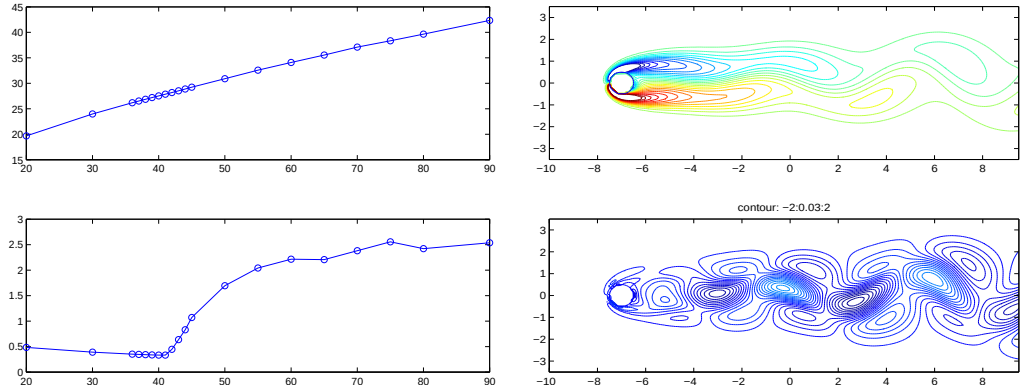

(a) (b)

Figure 7: Sensitivity analysis for a rotating cylinder. (a) Plot of the vorticity and sensitivity strength versus the Reynolds number defined as $1/\mu$. (b) The vorticity and sensitivity plot at $t = 100$ which verified the critical Reynolds number at $Re = 43$.

relative position of the cylinder is fixed, we just need to replace the no-slip boundary condition with the prescribed velocity of the rotation in our algorithm. From Fig. 7(a), we see that the critical Reynolds number is around $Re^* = 1/\mu^* = 42$ which is smaller than that of the stationary case indicating a less stable flow in the wake of the rotating cylinder. In Fig. 7(b), we plot the vorticity and sensitivity plot at time $t = 100$ and $Re = 1/\mu = 43$ which verified our claim about the critical Reynolds number. We can see that the vortex shading has developed after wake of the rotating cylinder.

3.4 Two stationary cylinders

We carry out the sensitivity analysis for a uniform flow past two separated cylinders. The level set function is defined as follows

$$\varphi_1(x,y) = \sqrt{(x+7)^2+y^2} - 1, \quad \varphi_1(x,y) = \sqrt{(x-x_2)^2+y^2} - 1, \tag{3.2a}$$

$$\varphi(x,y) = \min\left\{\varphi_1(x,y),\ \varphi_2(x,y)\right\}. \tag{3.2b}$$

In Fig. 8, we show the sensitivity analysis for the two stationary cylinders. We show three different cases. In the first case (a), the two cylinders are centered at $(-7,0)$ and $(-4,0)$, respectively. They are considered as relatively close. We see that the critical Reynolds number is about $Re^* = 54$ which is larger than that of a single cylinder. As we increase the distance between two cylinders by one unit, we see that the critical Reynolds number increases by 10, see Fig. 8(b) for which the two cylinders are centered at $(-7,0)$ and $(-3,0)$ respectively. If we further increase the distance between two cylinders by another 3 units, the critical Reynolds number remains almost the same. In Fig. 8, the left plots are the strength of the vorticity and sensitivity versus the Reynolds number defined as $1/\mu$. The right plots are the vorticity and sensitivity plot at $t = 100$ and a Reynolds number that is close to the critical Reynolds number 54, 64, and 65 respectively.

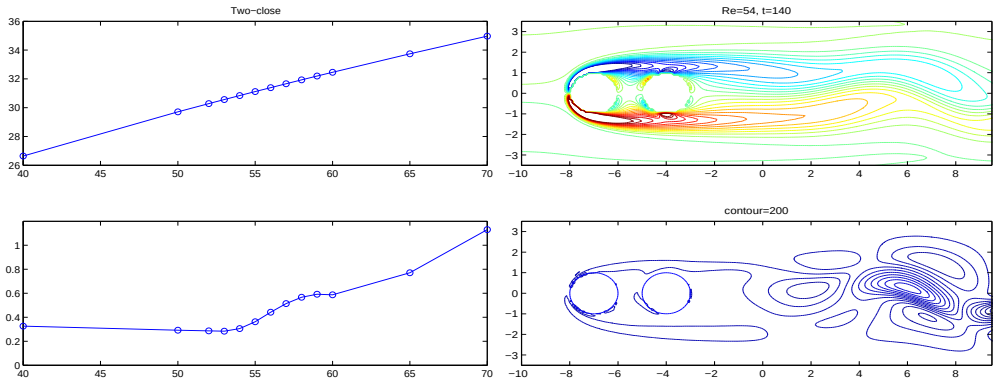

(a) Two cylinders centered at $(-7,0)$ and $(-4,0)$. The critical Reynolds is about 54.

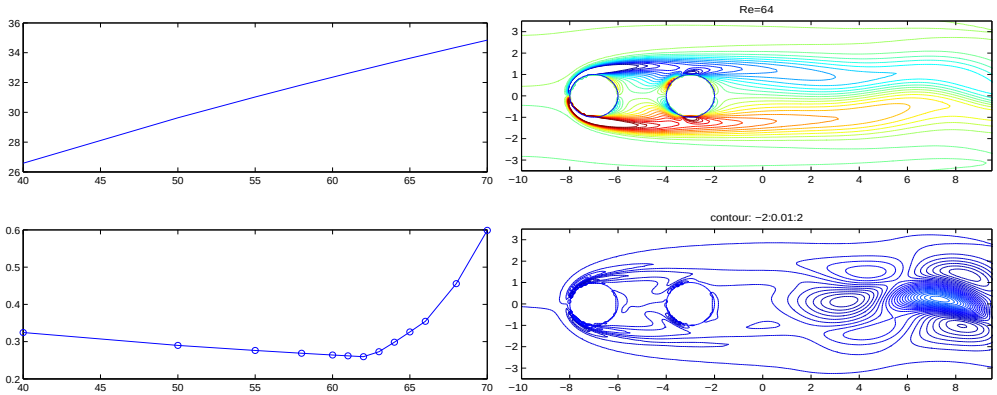

(b) Two cylinders centered at $(-7,0)$ and $(-3,0)$. The critical Reynolds is about 64.

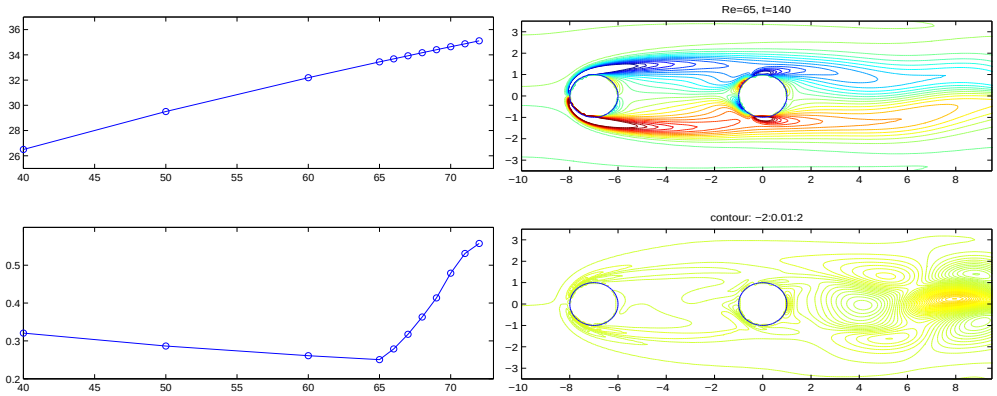

(c) Two cylinders centered at $(-7,0)$ and $(0,0)$. The critical Reynolds is about 65.

Figure 8: Sensitivity analysis of two stationary cylinders. The left plots are the strength of the vorticity and sensitivity versus the Reynolds number defined as $1/\mu$. The right plots are the vorticity and sensitivity plot at $t = 100$ and a Reynolds number that is close to the critical Reynolds number 54, 64, and 65 respectively.

We also tested the two rotating cylinders in the same, or different rotating directions with the same speed as above. The analysis in the wake of the second cylinder has similar behaviors as the stationary ones. But the flow patterns between the two

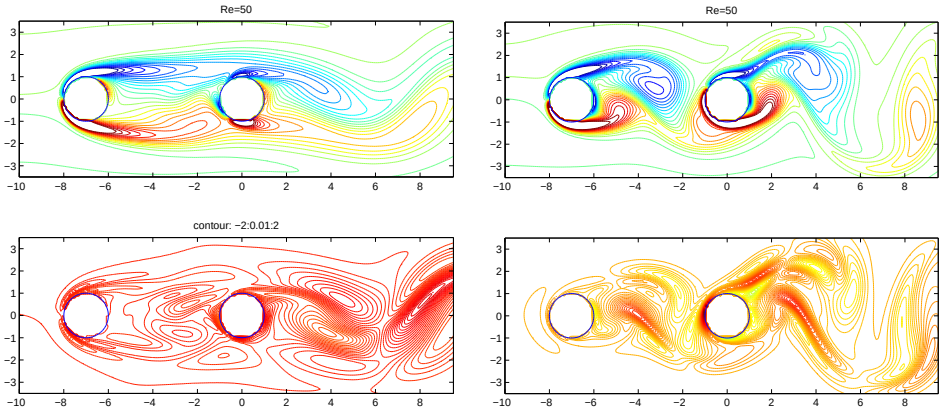

(a) (b)

Figure 9: Plot of vorticity (top) and sensitivity vorticity of two rotating cylinders at $t = 100$ and $Re = 50$. (a) Both cylinders rotate in the same direction (counter clockwise); (b) The two cylinders rotate in the opposite directions with the right one rotates in the counter clockwise direction.

cylinders are much affected by the directions of rotation. The flow between the two cylinders is more stable if the rotating directions are the same which means that the direction between the two cylinders are opposite. Otherwise it becomes less stable, see Fig. 9 in which we plot the vorticity and sensitivity vorticity for the two different cases at $t = 100$ and $1/\mu = 50$.

4 Conclusions

In this paper, we present the sensitivity analysis for flow past obstacles with respect to the Reynolds number. Such analysis enable us to predict the critical Reynolds number numerically. Various numerical experiments show such a prediction is reliable.

Acknowledgments

The first and second authors are partially supported by US-ARO grant 49308-MA, and US-AFSOR grant FA9550-06-1-0241. The second author is also partially supported by US-NSF grant DMS-0911434, and the US-NIH grant 096195-01, and CNSF 11071123. The third author is partially supported by the Hong Kong RGC Grant HKBU201710.

References

[1] J. B. Bell, P. Colella and H. M. Glaz, *A second-order projection method for the incompressible Navier-Stokes equations*, J. Comput. Phys., 85 (1989), pp. 257–283.
[2] D. L. Brown, R. Cortez and M. L. Minion, *Accurate projection methods for the incompressible Navier-Stokes equations*, J. Comput. Phys., 168 (2001), pp. 464–499.

[3] G. CACUCI, Sensitivity and Uncertainty Analysis, Vol. 1, Chapman & Hall/CRC, Boca Raton, FL, 2003.
[4] S. DENG, *Immersed Interface Method for Three Dimensional Interface Problems and Applications*, Ph.D thesis, North Carolina State University, 2000.
[5] S. DENG, K. ITO AND Z. LI, *Three dimensional elliptic solvers for interface problems and applications*, J. Comput. Phys., 184 (2003), pp. 215–243.
[6] A. G. GODFREY, *Sing sensitivities for flow analysis*, in Computational Methods for Optimal Design and Control, pages 181–196, Birkhauser, Boston, MA, 1998.
[7] J. HUNTER, Z. LI AND H. ZHAO, *Autophobic spreading of drops*, J. Comput. Phys., 183 (2002), pp. 335–366.
[8] K. ITO, Z. LI AND M-C. LAI, *An augmented method for the Navier-Stokes equations on irregular domains*, J. Comput. Phys., 228 (2009), pp. 2616–2628.
[9] K. ITO AND Z. QIAO, *A high order compact MAC finite difference scheme for the Stokes equations: augmented variable approach*, J. Comput. Phys., 227 (2008), pp. 8177–8190.
[10] R. J. LEVEQUE AND Z. LI, *The immersed interface method for elliptic equations with discontinuous coefficients and singular sources*, SIAM J. Numer. Anal., 31 (1994), pp. 1019–1044.
[11] Z. LI, *The Immersed Interface Method-A Numerical Approach for Partial Differential Equations with Interfaces*, PhD thesis, University of Washington, 1994.
[12] Z. LI AND K. ITO, *The immersed interface method-numerical solutions of PDEs involving interfaces and irregular domains*, SIAM Frontier Series in Applied Mathematics, FR33, 2006.
[13] Z. LI, K. ITO AND M-C. LAI, *An augmented approach for Stokes equations with a discontinuous viscosity and singular forces*, Comput. Fluids, 36 (2007), pp. 622–635.
[14] Z. LI AND M-C. LAI, *The immersed interface method for the Navier-Stokes equations with singular forces*, J. Comput. Phys., 171 (2001), pp. 822–842.
[15] Z. LI, H. ZHAO AND H. GAO, *A numerical study of electro-migration voiding by evolving level set functions on a fixed cartesian grid*, J. Comput. Phys., 152 (1999), pp. 281–304.
[16] S. OSHER AND R. FEDKIW, Level Set Methods and Dynamic Implicit Surfaces, Springer, New York, 2002.
[17] J. A. SETHIAN, Level Set Methods and Fast Marching Methods, Cambridge University Press, 2nd edition, 1999.
[18] L. G. STANLEY AND D. L. STEWART, *Design sensitivity analysis: computational issues of sensitivity equation methods*, SIAM, Philadelphia, 2002.